Wave Dissipation in a Field of Floating Perforated Spherical Shells

L. Victoria Arciniega, Logan Galindo, and Kevin J. Maki
Department of Naval Architecture and Marine Engineering
University of Michigan, Ann Arbor, MI 48109 USA
Corresponding author email: kjmaki@umich.edu

1 INTRODUCTION

There is intense interest in the changing climate, and the ice in the Arctic plays a key role in the global energy balance. This part of the planet holds significant deposits of fossil fuel, humans are travelling to the northern latitudes for adventure tourism, and there are significant national interests to patrol where the borders of Asia, Europe, and North America meet. The open ocean meets the icy waters in a region called the marginal ice zone (MIZ). In this region the conditions have floating broken ice. As ocean waves propagate from the open ocean into the MIZ their amplitude is attenuated and this complex process of energy loss is important yet difficult to model. The broken ice in this region has complex ever changing shapes, it oscillates due to the wave motion and can collide and raft with other floes, or break into smaller pieces. Many studies have been performed to observe wave dissipation due to floating ice with the aim to model the damping phenomenon [1, 2], and this abstract is focused on using experiments to observe dissipation and contribute to uncovering and modeling the mechanism of wave attenuation.

2 EXPERIMENTS

2.1 Facility The experiments were performed in the wind-wave tank at the Aaron Friedman Marine Hydrodynamics Laboratory at the University of Michigan. This facility has dimensions of 35 m long by 0.7 m wide with a nominal water depth of 0.65 m. A wedge-type wavemaker is located at the south end of the tank, and a passive beach at the other. The wedge has a 45 deg front face and it oscillates vertically. The facility can generate wind at speeds up to 30 m/s in the direction of wave propagation, but calm-wind conditions were used for all measurements in this study.

The surrogate for broken ice is a perforated spherical shell. The shells are commonly known as Whiffle balls and they are widely available in the United States. Each ball has diameter $D = 70.51$ mm and the shell thickness is 1.85 mm. The material is made of polyethylene with specific gravity approximately 0.93, which is near that of ice. The ball has 26 holes of diameter 10.81 mm (see fig. 1).

Two sonic wave probes are used to measure the waves upstream and downstream of a raft of the floating shells (Senix model TSPC-30S1-232). The first probe is 13 m from the wave maker, and the second is 17.97 m from the wavemaker.

A raft of shells is formed by using flexible cord as a thread through a series of balls to form a ring that contains freely floating shells within it. The outer ring is affixed to the tank walls using suction cups that are clipped together with the cord. An image of the raft inside the tank is shown in fig. 1. Also shown in this figure is a drawing of the Whiffle ball, and a schematic of the tank. The raft has length L and width $W = 0.7$ m (which is the width of

the tank). The number of balls N (including those on the outer ring) are so that the packing density $C = ND^2/LW = 1$. In the image (fig. 1) there is a space of empty water inside the ring due to drift and wandering of the loose cords on the upstream and downstream transverse edges of the ring.

2.2 Test Matrix Tests are performed systematically by varying the incident wave amplitude a, wave period T, and length of the raft L. A total of 21 runs were completed. The wavemaker moves with stroke $s(t) = f(t)s_0 \sin(\omega t)$, where $f(t)$ is a ramp function that goes from zero to one over the first three seconds of the motion, and from one to zero over the last three seconds of the wavemaker motion.

Runs 1 through 7 use a wave period $T = 1$ s, and the wave amplitude varies from 26 to 7 mm. The resulting steepness is in the range $30 < \lambda/2a < 110$. Runs 8-14 are conducted by varying the period and stroke amplitude with the goal of keeping steepness constant. The resulting incident wave amplitudes are in the range $2.6 < a < 19.5$ mm which correspond to steepness of $50 < \lambda/2a < 90$. The final set of runs 15-21 are a repeat of runs 8-14 but the length of the raft is doubled. The raft length for runs 1-14 is $L = 2.032$ m, and for runs 15-21 $L = 4.064$.

3 RESULTS

Energy dissipation is analyzed in terms of two quantities, the transmission coefficient H, and the attenuation coefficient k_i, both of which depend on the wave amplitude at each wave probe (WP1 and WP2). A fast-Fourier transform is applied to a steady-state segment of each time record to extract the amplitude at both locations, a_1 and a_2.

The attenuation coefficient assumes the wave amplitude decays slowly in the ice field according to the model $a(x) = a_0 e^{-k_i x}$. The two wave amplitude measurements are used to solve for the unknown k_i. Note that the coordinate of x used in the model equation is the upstream and downstream positions of the edges of the raft (not the wave probe) since it is assumed that no damping occurs between the probe and the raft edge. The values of the transmission coefficien H and k_i are determined by

$$H = \left(\frac{a_2}{a_1}\right)^2 \qquad k_i = -\frac{\ln(a_2/a_1)}{L}.$$

Data are collected for 100 s for each run. A sample time-history is shown in fig. 2. In the bottom of this figure the data starting from 40 s are plotted for 10 periods to inspect the regularity of the wave signals.

The transmission coefficient is calculated for runs 1-7 and shown in the left of fig. 3. The period is 1 s. The wave steepness is calculated as $\epsilon = ka_1$. Error bars are shown by assuming the uncertainty in each elevation measurement is 0.5 mm. It is remarkable to see that over the larger range of steepness that the transmission coefficient is relatively constant.

The transmission coefficient for runs 8-21 is shown in the right side of fig. 3. Here it can be observed that as the incident wavelength increases, so does the transmission.

Finally the attenuation coefficient is shown in fig. 4. The coefficient decreases rapidly with increasing wave period, and the two sets of data for different raft length lie close to each other indicating the model equation is suitable to account for raft length on the damping process. Note that for the shortest period the waves are of very small amplitude, practically

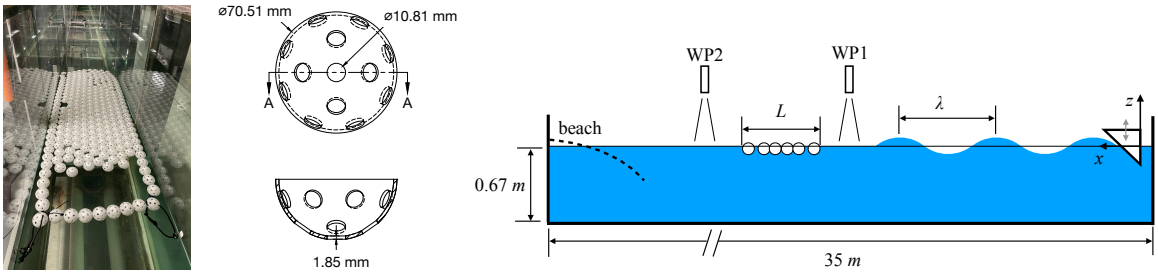

Figure 1: *(left)* Image of shells floating inside tank. *(center)* Drawing of perforated spherical shell. *(right)* Schematic of experimental facility.

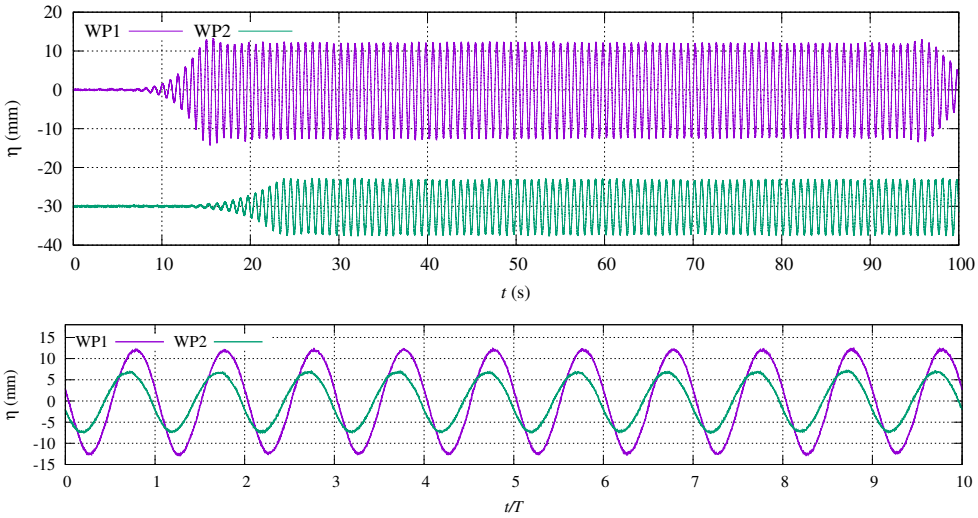

Figure 2: Time series from Run 10. *(top)* full time record over 100 s, data for wave-probe 2 shifted downward by 30 mm. *(bottom)* data series over 10 periods.

no energy propagates through the raft, and the measurement is dominated by uncertainty. In the right of fig 4 the value of k_i is plotted in log-log scaling as a function of the wave frequency.

Other work [3, 4] has suggested that the attenuation is a power law as a function of wave frequency. In fig. 4 lines according to the model $k_i \propto \omega^n$ are shown. [3] performs analysis on several different sets of field data that suggest $2 < n < 4$. For longer period the attenuation rate is closer to 2, and for shorter period it is closer to 4. Interestingly, the present data are at a much lower periods at laboratory scale, and the value of $n \approx 4$ is consistent with the lowest period field data. The lower period data are at a lower Reynolds number, and there may be a transition between laminar and turbulent flow that influences the rate of attenuation.

4 ACKNOWLEDGEMENTS

This work is supported by the Naval Engineering Education Consortium (NEEC). The authors would also like to acknowledge and thank the NEEC students, and research staff Jim Smith, and Jason Bundoff, all of whom were instrumental in setting up and performing the

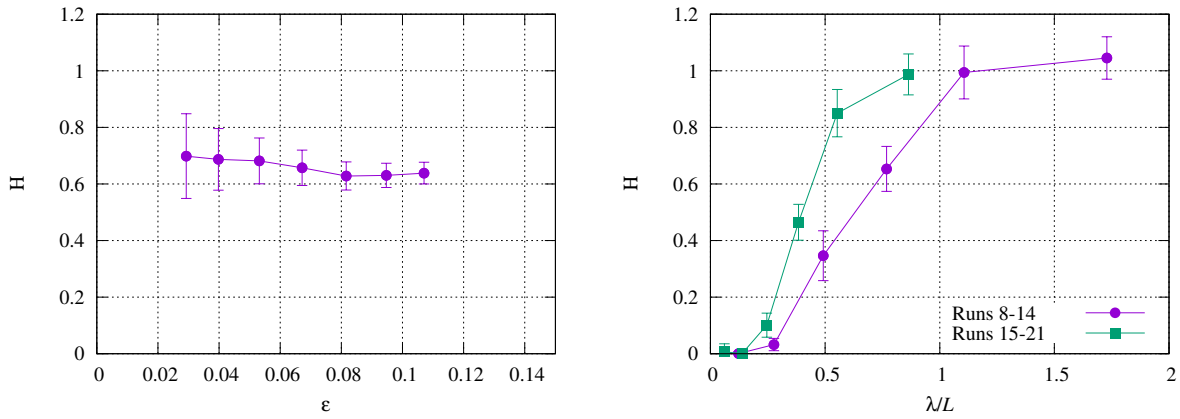

Figure 3: *(left)* Transmission for runs 1-7 where period is 1.0 s. *(right)* runs 8-21.

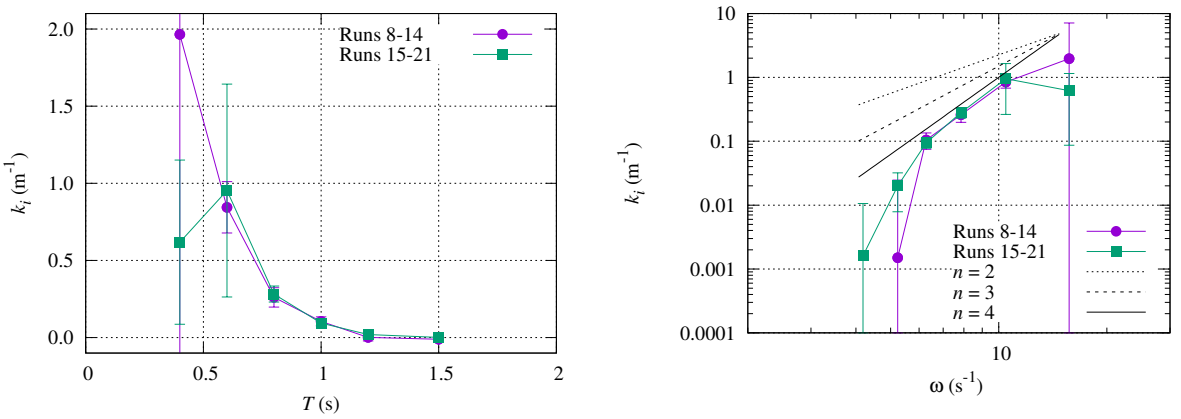

Figure 4: *(left)* Attenuation coefficient as function of period. *(right)* Log-log plot of attenuation as function of frequency with models of the form $k_i \propto \omega^n$.

experiments.

5 REFERENCES

[1] Toffoli, A., Pitt, J., Alberello, A., and Bennetts, L. 2022. *Modelling attenuation of irregular wave fields by artificial ice floes in the laboratory.* Philosophical Transactions of the Royal Society A 380(2235), 20210255.

[2] Rabault, J., Sutherland, G., Jensen, A., Christensen, K. H., and Marchenko, A. 2019. *Experiments on wave propagation in grease ice: combined wave gauges and particle image velocimetry measurements. Journal of Fluid Mechanics 864*, 876–898.

[3] Meylan, M. H., Bennetts, L. G., Mosig, J., Rogers, W., Doble, M., and Peter, M. A. 2018. *Dispersion relations, power laws, and energy loss for waves in the marginal ice zone.* Journal of Geophysical Research: Oceans 123(5), 3322–3335.

[4] Rogers, W. E., Meylan, M. H., and Kohout, A. L. 2021. *Estimates of spectral wave attenuation in Antarctic sea ice, using model/data inversion. Cold Regions Science and Technology 182*, 103198.